Numerical Simulations of Cavity Effects on Thrust Oscillations in Subscale Solid Rocket Motors

Stany GALLIER
SNPE Matériaux Energétiques, 91710 Vert-le-petit, France

Michel PREVOST
ONERA, 31410 Mauzac, France

ABSTRACT

Aeroacoustic instabilities in subscale solid rocket motors are studied by a combined experimental/numerical approach. The present work intends to focus on how these instabilities can be modified by rocket internal geometry, especially the presence of cavity. Numerical simulations are performed on several subscale rocket motors that have been experimentally fired. Computations and measurements are often in correct agreement, which helps to clarify the role of cavities. In particular, aft-cavities due to nozzle submergence involve significant acoustic production and favor instabilities. The role of large central cavities seems however more complex and has not been cleared up yet.

1. INTRODUCTION

Most large solid rocket motors (SRM) are reported to exhibit instabilities during operation. These instabilities become apparent as thrust oscillations that involve vibrations detrimental to carrying load. During past years, active research on instabilities on large motors showed that they are mostly dominated by a coupling between chamber acoustics and hydrodynamic instabilities. The latter arise from a vortex shedding stemming either from an unstable shear layer (caused by a protruding inhibitor for instance), or from the Taylor flow intrinsic instability. This instability, so-called PVS (Parietal Vortex Shedding), has been supported by experimental [1], numerical [2] or analytical studies [3] and is found to be a powerful source of instability in large SRM.

The present work intends to study how such aeroacoustic instabilities are altered by the rocket internal geometry, especially the presence of cavity. This cavity may appear between segments (slots in segmented grains) or from nozzle integration for instance. Indeed, it has been previously noted that the aft-cavity induced by a submerged nozzle can strongly enhance the instability levels in cold-flow experiments [4,5]. Likewise, some recent numerical simulations on a subscale solid rocket motor have showed that a large central cavity can dramatically lower pressure oscillations [6].

In order to improve prediction and design capabilities, it seems crucial to improve the knowledge of the underlying physics, through a coupled numerical/experimental approach.

2. EXPERIMENTAL RESULTS

The present work focuses on several subscale motors, so-called LP-9, that have been fired in ONERA, Toulouse, during the last few years. Such LP9 motors are typically 0.7 m long and are loaded with a non-metallized AP/HTPB solid propellant (~ 2 kg). Burning time is about 2.5 s for an average pressure around 5 MPa. Unsteady pressure is measured by piezoelectric transducers at different locations and data are then processed using Hilbert transforms to obtain the instability levels and frequencies.

More than thirty LP9 motors have been fired so far and the present study will focus only on four of them. The considered configurations will differ from either grain geometry (single-segment or segmented with central slot) or nozzle integration, in order to investigate the effects of cavities. They are displayed in Tab.1 with a sketch of the geometry and the measured instability pressure level (non-dimensional in time and pressure, same scale).

Configuration	Sketch	Instability pattern
0	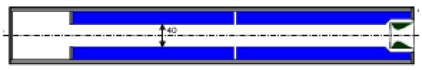	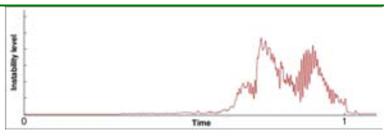
1		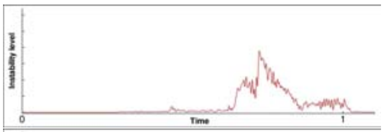
2		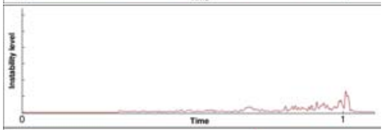
3		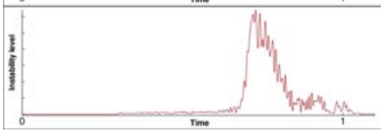

Tab. 1: Considered LP9 configurations

- Configuration #0 is chosen as the reference case. It has a segmented grain, with a central slot, and a submerged nozzle. This motor is unstable and exhibits three instability bursts during the latter half of firing.

- Configuration #1 intends to estimate the role of the nozzle submergence. The nozzle is now mounted back while the grain of configuration #0 is conserved (segmented, cylindrical with an aft recessing). The instability pattern is quite similar to the previous reference case except that the third burst has now disappeared.

- Configuration #2 keeps the previous non-submerged nozzle but the grain is now cylindrical (no recessing). This motor is virtually stable.

- Configuration #3 is similar to the baseline configuration #0 but has a no central slot (single-segment grain). The unstable behavior is significantly modified, as one single instability burst is measured.

For these four configurations, instabilities are experimentally locked on the first longitudinal acoustic mode. More details on experiments may be found in [7,8].

3. NUMERICAL SIMULATIONS

3.1 Firing restitutions

Prior to computations, a zero-dimensional steady-state restitution is carried out. It involves computing the theoretical surface and pressure history that are compared with the experimental pressure to fit the actual burning rate accounting for scale and hump effects. As an example, Fig. 1 displays the experimental and theoretical pressure for the baseline configuration #0.

At this stage, this approach can be used to define the actual geometry and propellant rate for any desired time to be investigated by further computations. As a general rule, the times (and associated geometry) selected for computations are chosen to comply with the occurrence of the maximum instability levels noted in measurements.

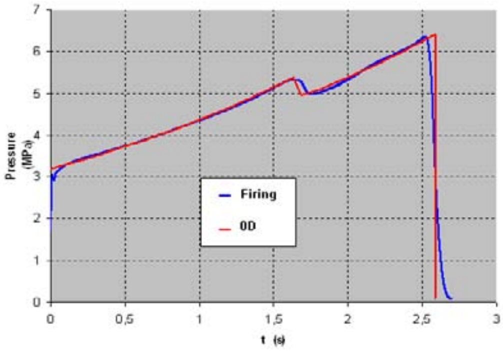

Fig. 1: Measured and theoretical pressure (config. #0)

3.2 Numerical simulations

Computations are performed within a 2D axisymetric assumption using a house-in CFD code (CPS) from SNPE. Compressible unsteady Navier-Stokes equations are solved with additional perfect gas equation of state. The code adopts a finite-volume technique on unstructured mesh. Conservative variables are calculated at the center of each computational cell whereas convective fluxes are computed at cell edges using an approximate Riemann solver (Roe scheme), second-order accurate in space. Temporal integration is achieved using an explicit two-step Runge-Kutta algorithm.

Turbulence is accounted for using a non-linear URANS approach (Haminh-Kourta model [9]). This model conceptually decomposes any instantaneous variable into coherent organized and incoherent random parts by phase-averaging. Original model from Ref. [9] is based on a Jones-Launder k-ε model but has been here recast in a q-ω frame to keep benefit of the ω-equation in wall regions (see Ref. [6] for model details). Additionally, a large-eddy simulation (LES) technique has been used for one configuration (#2). In this case, a classical Smagorinsky subgrid model is chosen.

Numerical simulations have also been conducted without turbulence modeling, just in order to gauge the effects of turbulence. As a general rule, turbulence lowers instability levels, typically by 30 to 50 % depending on the case. This means that turbulence has a significant role for these configurations.

Only single-phase flow will be assumed in the following computations because the propellants used do not contain any aluminum.

Boundary conditions for the gas injection -modeling the propellant combustion- are an imposed mass flux, energy flux and zero tangential velocity (normal injection). For present computations, the propellant burning rate r_b follows a classical Vieille's law: $r_b=a_b p^n$ with n=0,3 and a_b estimated by the previous steady-state restitution. Propellant flame temperature is set to T_f=2320 K. Injected turbulence is computed with a suitable wall model that reconstructs the near-wall flow between injecting wall and first cell and estimates the turbulent variables via a specific mixing length model.

Computations are conducted on a fixed geometry (i.e., non-moving) because burnback time scales are very large compared to aerodynamic or acoustic time scales. As specified previously, different times (and associated geometry) have to be selected for numerical investigations. The study will focus on the second and third burst of the reference case (see instability pattern in Tab. 1). The corresponding times will also be considered for the other configurations.

The computational grids typically involve about 130,000 elements and they are kept relatively similar between configurations in order to reduce mesh effects. Such a grid includes roughly 1200 points in the axial direction (motor length) and about 100 points in the radial direction. The grid is clustered near the propellant surface. *A posteriori* examinations of the y^+ values confirm the relevance of this mesh for turbulent computations. Grid convergence has also been checked. Figure 2 shows the mesh for the reference case #0. This geometry corresponds to the maximum instability of the second burst. An

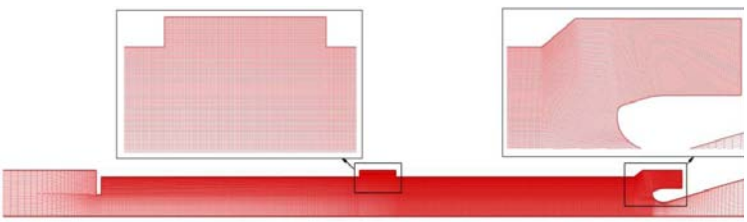
Fig. 2: Mesh for configuration #0 (second burst time)

important grid point density can be noticed in the central slot and in the aft-cavity.

4. RESULTS AND DISCUSSION

4.1 Effects of nozzle integration and aft cavities

In this section, the results obtained on configurations #0 and #1 are considered (see Tab.1). For these cases, the computations have been conducted at the same physical time. Figure 3 presents the computed instability levels (at motor head-end), as well as the experimental levels, for the reference case #0. Results are graphed with respect to the non-dimensional time t/t_{burn} where t_{burn} is the burning time, so that $t/t_{burn}=1$ corresponds to the end-of-burning. Instability prediction is globally correct with a fairly good estimation for the second burst even though an underestimation for the third burst can be noticed. As stressed previously, turbulence seems to play a role and discrepancies -like the relevance of the turbulence model or the injected rate of turbulence- are expected to slightly affect the computed pressure levels.

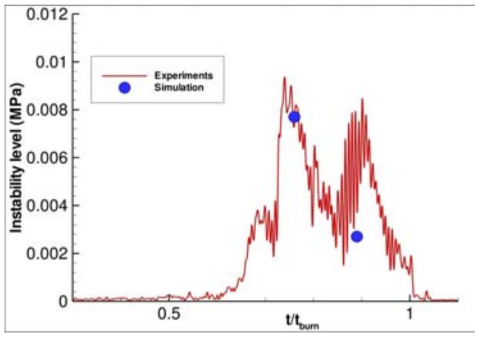

Fig. 3: Instability prediction (config. #0)

The computed instability frequency matches the measured frequency (700 Hz) suggesting that the first longitudinal acoustic mode is locked on. Figure 4 displays a map of the vorticity that clearly shows that the instability is driven by a Parietal Vortex Shedding. The typical vortical structures of this instability are noticed to take place by the beginning of the second segment, downwind the central slot.

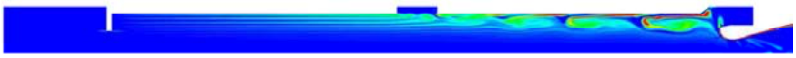

Fig. 4: Vorticity contours (config. #0)

Figure 5 shows the predictions for configuration #1, when the nozzle is now moved back (non-submerged) while the grain is kept identical (including the recessing, see Tab. 1). The first two instability bursts are rather similar and this seems to be well predicted by the computations for the second burst. However, the third burst has now virtually vanished which proves that this last burst is caused by the nozzle submergence. This effect is well reproduced by the simulations: the motor is now predicted to be stable.

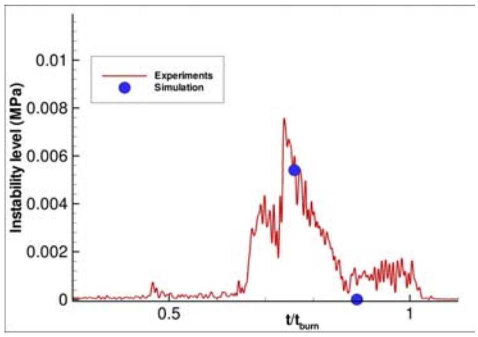

Fig. 5: Instability prediction (config. #1)

The reasons of this stability by the end of burning can be elucidated upon the examination of the aerodynamic fields (Fig. 6). This figure presents the vorticity contours in the aft-part of the motor, as well as the streamlines. For configuration #0, an aft-cavity is induced by the presence of the submerged nozzle. This aft-cavity is known to produce significant acoustic power as shown by Anthoine [4,5]. His analysis was based on the Howe acoustic analogy [10], that shows that the produced acoustic power is proportional to $\int_V (\boldsymbol{\omega} \times \mathbf{v}).\mathbf{u}'\, dV$ where $\boldsymbol{\omega}$, $\mathbf{v}$, $\mathbf{u}'$ are

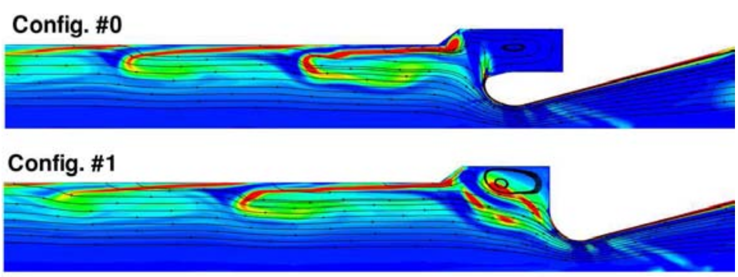

Fig. 6: Vorticity contours and streamlines (config. #0 and #1)

the vorticity vector, mean velocity vector, and acoustic velocity vector, respectively. When the vortices travel in front of the cavity entrance, the acoustic velocity vector $\mathbf{u}'$ (normal to cavity entrance) is almost normal to the vortex path, which creates sound.

For configuration #1, Fig.6 shows that the recessing acts like a step and involves a recirculation bubble. Likewise, this creates a misalignment between vortex path and acoustic velocity, so that, from an aeroacoustic viewpoint, this recirculation may be seen as a cavity. This clarifies the similarity of the instability pattern between these two configurations. However, as the propellant burns back, the step from the recessing is getting smaller and, by the end of burning, is too small for a recirculation to take place. This explains the absence of instability by the end of firing and stresses the role of the aft-cavity.

4.2 Effects of central cavities

Although this configuration is not presented, a LP9 motor with a cylindrical grain and without aft-cavities would be unstable due to a parietal vortex shedding [1-3].

Therefore, configuration #2 intends to analyze the effects of a central cavity by considering a motor devoid of aft-cavities (neither recessing nor nozzle submergence) but with a central slot due to a segmented grain (see Tab. 1).

This configuration is surprisingly stable for the whole firing (Fig. 7). On the contrary, the computations suggest that the motor remains unstable, even though the instability level is predicted to be slightly lower compared to the previous configurations. Only a single geometry has been considered but, although this should be checked, other times are expected to be unstable too.

This clearly points out that large central cavities may hinder the development of a vortex shedding in some cases. In Ref. [6], some simulations on another subscale motor with a large central cavity led to the same conclusions. The reason of this stabilizing role of the cavity is not clearly understood at the moment. It may be suggested that a large cavity can enhance turbulence effects.

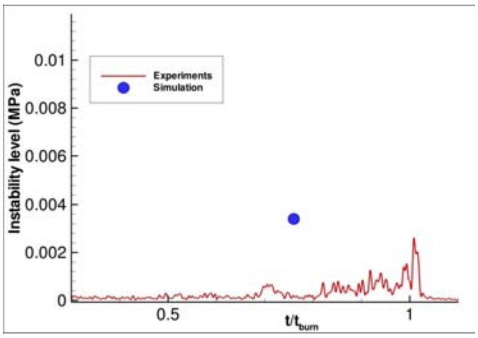

Fig. 7: Instability prediction (config. #2)

In order to validate this assumption, additional computations have been carried out. First, the former simulation has been resumed but with a much larger grid (500,000 cells), extremely refined around the cavity region, but this did not alter much the results. Then, a 3D detailed simulation was performed by computing this configuration with a LES model on a mesh with 6.2 million cells. As seen on Fig. 8, the parietal vortex shedding is still present and does not seem to be affected by the cavity. Instability levels are roughly similar to 2D simulations and the flow remains axisymetric.

At this stage, it is interesting to notice that a segmented configuration without aft-cavity is quite complex and its behavior remains difficult to be reproduced by present simulations. On the other hand, the previous configurations #0 and #1 do indeed have a central cavity and are found to be correctly predicted. This surely means that aft-cavities are a powerful source of instabilities, at least powerful enough to compensate the stabilizing role of the central cavity.

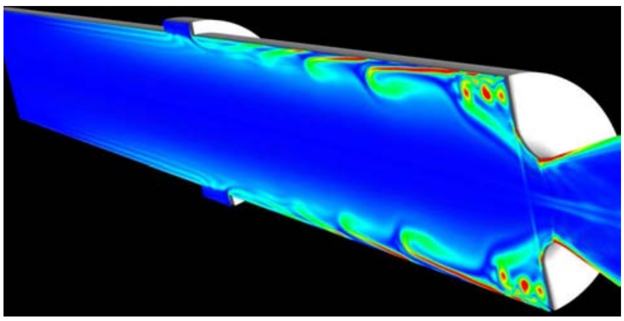
Fig. 8: Vorticity contour (config. #2)

From this viewpoint, it is interesting to consider the last configuration #3. It is basically the reference case #0 but with a single-segment grain, i.e. without central cavity. Computed and experimental instability levels are presented in Fig. 9. The interesting feature is that the removal of the central cavity modifies the instability pattern, as there is now a single important burst. This seems to be well recovered by the computations that also confirm the absence of a third burst. This basically means that in some cases, the cavity can also promote the instability. Actually, computations suggest that, without cavity, the vortices spring up in the very aft region of the motor and are much less developed (Fig. 10). The comparison between Fig. 10 and Fig. 4 stresses this difference quite obviously. The central cavity is here suspected to trigger the vortex shedding.

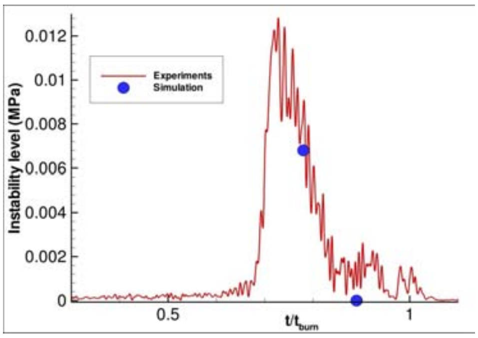

Fig. 9: Instability prediction (config. #3)

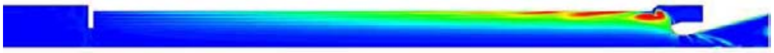
Fig. 10: Vorticity contours (config. #3)

5. CONCLUSIONS

This work presented a comparison between simulations and experimental measurements concerning the stability of subscale solid rocket motors. The purpose was to understand better to what extent the rocket internal geometry (in particular central slot or nozzle integration) can alter stability.

Simulation results show that the considered motors are dominated by a parietal vortex shedding. In most cases, computations -with turbulence modeling- are in good quantitative agreement with the experiments in terms of pressure oscillation levels, which helps to understand better the underlying physics. It is for instance found that the nozzle submergence favors aeroacoustic instabilities due to the persistent presence of an aft-end cavity. Some aft-end cavity due to grain design (recessing) can similarly induces significant instability levels due to the formation of a recirculation bubble, but only at the early stages of burning.

The role of large central cavities is however less clear and more complex to predict. On one hand, computations and experiments suggest that this cavity is liable to trigger the parietal vortex shedding, thereby favoring unstable conditions (configuration #3). On the other hand, central cavity might sometimes hinder the instability development (configuration #2). At this moment, it is not clear where this stabilizing behavior comes from, even though turbulence effects are suspected. Yet, a 3D LES simulation did not bring new insights and it is believed that an improved knowledge of turbulence in solid rocket motors is mandatory if one wants to provide a detailed scenario on the exact role of central cavities.

6. REFERENCES

[1] Avalon, G., Casalis, G. and Griffond, J., “Flow Instabilities and Acoustic Resonance of Channels with Wall Injection”, AIAA Paper 98-3220, July 1998

[2] Lupoglazoff, N., and Vuillot, F., “Parietal Vortex Shedding as a Cause of Instability for Long Solid Propellant Motors”, AIAA Paper 96-0761, Jan. 1996

[3] Chedevergne, F., Casalis, G., and Féraille, T., “Biglobal Linear Stability of the Flow Induced by Wall Injection”, *Phys. Fluids*, 18 (1), 2006

[4] Anthoine, J., Buchlin, J.-M., Guéry, J.-F.,” Experimental and Numerical Investigations of Nozzle Geometry Effect on the Instabilities in Solid Propellant Boosters”, AIAA Paper 2000-3560, July 2000

[5] Anthoine, J. and Lema, M., “Passive Control of Pressure Oscillations in Solid Rocket Motors: Cold-Flow Experiments”, *J. Prop. Power*, 25 (3), 2009

[6] Gallier, S., Godfroy, F., Plourde, F. “Computational Study of Turbulence in a Subscale Solid Rocket Motor”, AIAA Paper 2004-4052, 2004
[7] Prevost, M., Godon, J.C., Innegraeve, O., “Thrust Oscillations in Reduced Scale Solid Rocket Motors Part I : Experimental Investigations”, AIAA Paper 2005-4003, July 2005
[8] Prevost, M., Hijlkema, J., Gallier, S., and Roumy, M., “Effects of Cavity on Thrust Oscillations in Subscale Solid Rocket Motors”, AIAA-2009-5253, Aug. 2009
[9] Kourta, A., “Computation of Vortex Shedding in Solid Rocket Motors Using Time-Dependant Turbulence Model”, *J. Prop. Power*, 15(3), 1999
[10] Howe, M., “The Dissipation of Sound at an Edge”, *J. Sound Vib*., 70, 1980